Persistent magnetism in silver-doped BaFe$_2$As$_2$ crystals

Li Li,[1] Huibo Cao,[2] David S. Parker,[1] Stephen J. Kuhn,[1,3] and Athena S. Sefat[1]

[1]*Materials Science & Technology Division, Oak Ridge National Laboratory, Oak Ridge, Tennessee 37831, USA*

[2]*Quantum Condensed Matter Division, Oak Ridge National Laboratory, Oak Ridge, Tennessee 37831, USA*

[3]*Department of Physics, University of Notre Dame, Notre Dame, Indiana 46556, USA*

We investigate the thermodynamic and transport properties of silver-substituted BaFe$_2$As$_2$ (122) crystals up to $\sim$4.5%. Similar to other transition-metal substitutions in 122, Ag diminishes the antiferromagnetic (T_N) and structural (T_S) transition temperatures, but unlike other electron-doped 122s, T_N and T_S coincide without splitting. Although magnetism drops precipitously to $T_N = 84$ K at doping $x = 0.029$, it only weakly changes above this x, settling at $T_N = 80$ K at $x = 0.045$. Compared to this persistent magnetism in Ag-122, doping other group 11 elements of either Cu or Au in 122 diminished T_N and induced superconductivity near $T_c = 2$ K at $x = 0.044$ or 0.031, respectively. Ag-122 crystals show reflective surfaces with surprising thicker cross sections for $x \geqslant 0.019$, the appearance that is in contrast to the typical thin stacked layered feature seen in all other flux-grown x122 and lower Ag-122. This physical trait may be a manifest of intrinsic weak changes in c lattice and T_N. Our theoretical calculations suggest that Ag doping produces strong electronic scattering and yet a relatively small disruption of the magnetic state, both of which preclude superconductivity in this system.

I. INTRODUCTION

High-temperature superconductivity (HTS) is the most mysterious and elusive property in condensed-matter physics found in two Cu- and Fe-based material families [1,2]. The iron-based superconductors (FeSC) share some common features with the cuprates [3,4], most importantly that the superconducting state is triggered by chemical doping (or pressurizing) of an antiferromagnetic (AF) parent material [3–6]. On the other hand, the parents of FeSC have Fermi surfaces that are sensitive to small changes in composition [7–9], and certain applications of pressure [6] or chemical substitutions [10] in the Fe plane can instigate superconductivity. In FeSC (see Refs. [4,11–22] for several reviews), there is a highly complex interplay of factors, such as competition between magnetism and superconductivity, close proximity of lattice distortion to the T_N and the associated nematicity, orbital ordering, local moment, twinning, disorder, and chemical clustering. Despite the rich physical chemistry that FeSC offers [23] and the vast experimental and theoretical work seen in review manuscripts [24–29], many things about them remain unpredictable (e.g., chemistry doping trends, reasons for HTS, and the particular T_N and T_c values).

The BaFe$_2$As$_2$ transitions from tetragonal ($I4/mmm$) non-magnetic (NM) state into orthorhombic ($Fmmm$) striped-AF phase below $T_S = T_N = 132-134$ K (flux-grown crystals) [30,31]. For 122, transition-metal doping with either holes (e.g., 3d Cr, Mn; 4d Mo) [32–35] or electrons (e.g., 3d Co, Ni; 4d Rh, Pd) [10,36–38] suppresses AF, but only electron dopants can instigate superconductivity. The reason for this is not exactly solved, especially since the dopants can be very low in concentration (<8%). However, a couple of trends are noted in the literature. One, electron doping using 3d or 4d in the same group (Co and Rh or Ni and Pd) gives overlapping temperature-composition ($T - x$) phase diagrams [39]. However, this breaks for 5d, where Pt-122 gives a much wider x superconducting region ($x \approx 0.01$ to 0.11) [40,41]; moreover, Ir-122 shows $T_c \sim 26.4$ K up to $x = 0.20$, which

implies an even wider superconducting dome [42]. Two, for electron doping using Co [43,44], Ni [45], Rh [38,46], Pd [38], Ir [47], or Cu [37], the T_S and T_N decrease while they decouple ($T_S > T_N$) with increasing x, eventually giving superconductivity. In contrast, both transitions happen at identical temperatures for all 122 hole-doping cases of Cr [35], Mn [33,48], and Mo [34], and no superconductivity emerges in them. This paper is the first case study of the effects of 4d Ag doping in BaFe$_2$As$_2$ (Ag-122), and we construct and compare the $T - x$ phase diagram to that of the closely related 3d Cu-122.

In this paper, we provide experimental evidence for the properties of Ag-122 crystals using the variety of temperature-dependent magnetization, resistivity, heat capacity, Hall effect, and neutron diffraction measurements. Comparing 4d Ag-122 to 3d Cu- and 5d Au- dopants of the same group, similar suppression of T_N is seen up to $x \sim 0.02$. However, while Cu- and Au-122 give superconductivity at $\sim$2 K at $x = 0.044$ [37] and 0.031 [49], respectively, Ag remains magnetic up to $x = 0.045$. Our results show that Ag substitution gives a coupled T_S/T_N feature similar to hole-doped nonsuperconducting 122s. Our density of state (DOS) calculations show that Ag creates essentially a band separate from the rest of the 122 electronic states, indicative of intense electronic scattering, different from that seen for superconductors such as Co- or Cu-122s.

II. EXPERIMENTAL RESULTS AND DISCUSSION

Single crystals of Ag-doped BaFe$_2$As$_2$ were grown out of FeAs self-flux technique [23]. To produce a range of dopant concentrations, small barium chunks, silver powder, and FeAs powder were combined according to various loading ratios of Ba : Ag : FeAs = 1 : x : 5 (listed in Table I) in a glove box, and each were placed in an alumina crucible. A second catch crucible containing quartz wool was placed on top of each growth crucible, and both were sealed inside a silica tube under $\sim$1/3 atm argon gas. Each reaction was heated for $\sim$24 h

TABLE I. For $Ba(Fe_{1-x}Ag_x)_2As_2$, loading reaction ratio (Ag:FeAs), and silver amount found from EDS (x); room-temperature lattice parameters refined from x-ray diffraction data; summary of transition temperatures inferred from resistivity, magnetization and specific heat measurements, and neutron results.

| | | | | T_N, T_s (K) | | | |
Ag: FeAs	x	c(Å)	a(Å)	(dR/dT)	$(d\chi/dT)$	(dC/dT)	(neutrons)
0:5	0	13.0151(3)	3.9619(2)	132	132	132	133
0.1:5	0.005	13.0236(6)	3.9647(2)	120	120	120	125
0.2:5	0.009	13.028(1)	3.9668(4)	114	108	111	–
0.3:5	0.016	13.029(1)	3.9685(3)	106	106	106	105
0.4:5	0.019	13.029(1)	3.9714(3)	101	96	100	–
0.5:5	0.026	13.037(1)	3.9736(3)	90	92	93	93
0.6:5	0.029	13.0389(6)	3.9749(2)	76	86	–	84
0.7:5	0.035	13.0367(8)	3.9775(2)	80	82	–	80
0.9:5	0.040	13.0363(4)	3.9789(3)	79	79	–	–
1.1:5	0.045	13.0398(6)	3.9801(1)	75	79	–	80

at 1180 C and then cooled at a rate of 1 to 2 °C/h, followed by a decanting of the flux around 1050 °C. The crystals were flat with dimensions of $\sim 6 \times 4 \times 0.1\,mm^3$ or smaller. Similar to 122 [36], the crystals of Ag-122 formed with the [001] direction perpendicular to the flat faces. Attempts for higher Ag contents were unsuccessful and led to only inhomogeneous phase. The chemical composition of each crystal batch was measured with a Hitachi S3400 scanning electron microscope operating at 20 kV; energy-dispersive x-ray spectroscopy (EDS) indicated that significantly less Ag is chemically substituted in the 122 structure than put in solution. Three spots ($\sim 80\,\mu$m) were checked and averaged on each random crystalline piece; the crystals had the same composition within each batch within error; no impurity phases or inclusions were detected. The samples are denoted by measured EDS x values (each x with a relative uncertainty of 5%) in $Ba(Fe_{1-x}Ag_x)_2As_2$ throughout this paper (Table I). Although Ag-122 crystals have similar flat crystalline faces along the ab plane [marked by green arrows in Fig. 1(a)], they exhibit two different crystalline features in cross section [marked by yellow arrows in Fig. 1(b)]. For $0 \leqslant x < 0.019$, the cross section clearly shows a stacked layered feature, while for $0.019 < x \leqslant 0.045$ the cross section displays a uniform reflective surface with a nonlayered feature. We have not seen such thicker cross-sectional features in other doped 122 systems.

Bulk phase purity of Ag-122 crystals was checked by collecting data on an X'Pert PRO MPD x-ray powder diffractometer using monochromatic Cu $K_{\alpha 1}$ radiation in the $10-70°$ 2θ range, on ground crystals, each weighing ~ 30 mg collectively. Lattice parameters were refined from full-pattern refinements using X'Pert HighScore Plus software. The Bragg reflections were indexed using the tetragonal $ThCr_2Si_2$ tetragonal structure ($I4/mmm$), with no impurity phases. The refined lattice constants are listed in Table I; Fig. 1(c) plots a and c lattice parameters as a function of x for Ag-122. With Ag doping, the lattice parameter c first increases at $x < 0.01$, then exhibits a step-shape jump at $x = 0.019$ and remains nearly unchanged above. However, the lattice parameter a keeps increasing linearly up to the doping limit $x = 0.045$, which is consistent with the effective substitution of Ag into system, reflected in cell volume expansion with x [Fig. 1(c), inset]. Compared to 122, a increases by 0.39% for Ag-122 at

$x = 0.035$, a larger change than the 0.22% for Cu-122 at same x [37]; moreover, Ag doping also expands c, in contrast with Cu doping. For Co-122, both a and c decrease monotonically. The different doping effects on the 122 lattice should be related to ionic radii variations, assuming +2 oxidation states, i.e., Ag^{2+}(94 pm) $>$ Fe^{2+}(78 pm) $>$ Co^{2+}(74 pm) $>$ Cu^{2+}(73 pm) [50].

Magnetization measurements for $Ba(Fe_{1-x}Ag_x)_2As_2$ were performed in a Quantum Design (QD) Magnetic Property Measurement System (MPMS). For a temperature-sweep
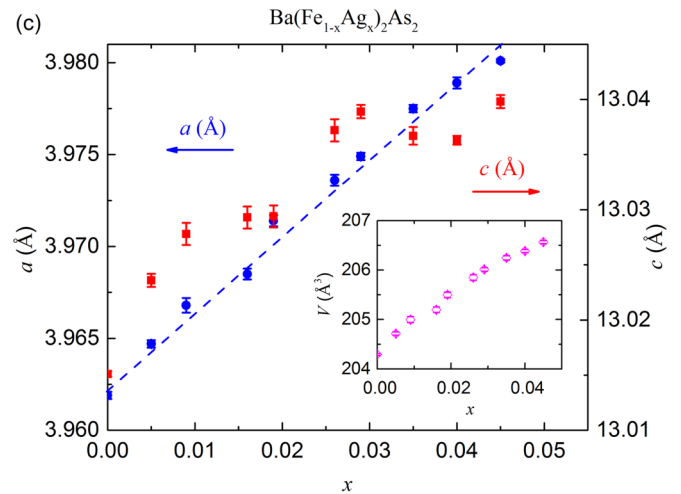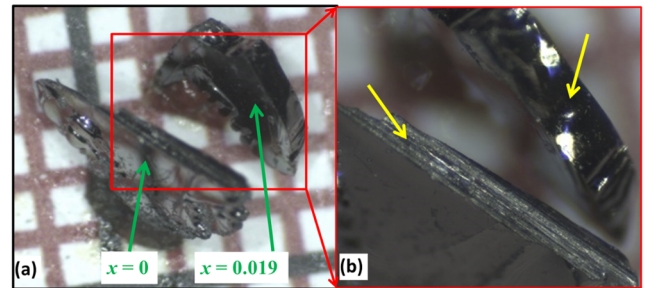

FIG. 1. (a) Typical single crystals for $x = 0$ and 0.019. (b) Enlarged view for the cross section of $x = 0$ and 0.019 crystals. (c) Refined lattice parameters for $0 \leqslant x \leqslant 0.045$ in $Ba(Fe_{1-x}Ag_x)_2As_2$ series; inset is cell volume V vs x.
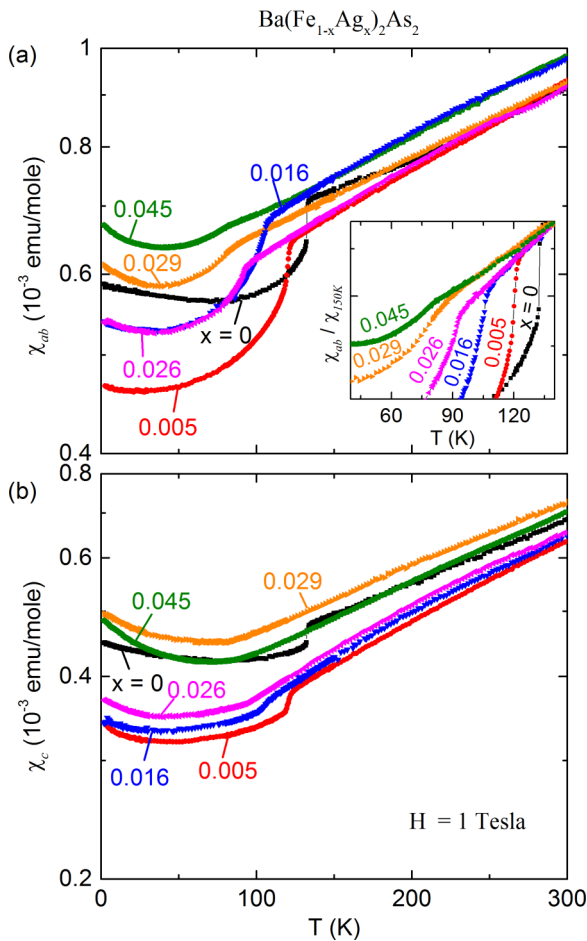
Ba(Fe$_{1-x}$Ag$_x$)$_2$As$_2$

FIG. 2. For Ba(Fe$_{1-x}$Ag$_x$)$_2$As$_2$, temperature dependence of magnetic susceptibility for the range of $0 \leqslant x \leqslant 0.045$, (a) along ab and (b) c lattice directions. Inset of (a) displays the normalized results along the ab direction in the temperature range of $40\,\mathrm{K} \leqslant T \leqslant 140\,\mathrm{K}$.

experiment, the sample was cooled to 2 K in zero field (ZF), and data were collected by warming from 2 to 300 K in an applied field of 1 Tesla. Figures 2(a) and 2(b) present the magnetic-susceptibility results along ab and c crystallographic directions. For BaFe$_2$As$_2$, the susceptibility decreases approximately linearly with decreasing temperature and then drops abruptly below $T_N = T_S \approx 132$ K, reproducing the well-established behavior [30,31]. There is a small anisotropy difference at room temperature between χ_{ab} and χ_c. In the entire doping series, all the absolute values of χ_{ab} are larger than χ_c at room temperature. However, for all Ag-122 above ~ 150 K, the susceptibility data nearly display comparable linear dependence; they are neither Pauli- nor Curie-Weiss-like behavior, attributed to the multiband nature of FeSCs and the spin-density-wave (SDW) nature of local and itinerant electrons [51]. For $0 \leqslant x \leqslant 0.026$, $\chi(T)$ displays similar temperature behavior, although the transition temperatures are reduced with x. For $x = 0.005, 0.009, 0.016, 0.019$, and 0.026, T_N values are inferred as ≈ 120 K, 108 K, 106 K, 96 K, and 92 K, respectively, using the χ derivative method, as in Ref. [37]. The full list for these values is summarized in Table I. For $x \geqslant 0.029$ crystals, the change in T_N is small, and the transitions are not as sharp as in the 122 parent [Fig. 2(a), inset].
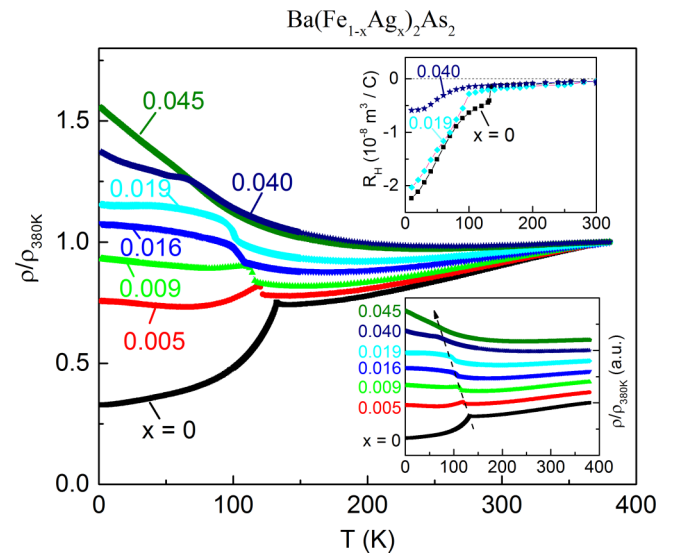
Ba(Fe$_{1-x}$Ag$_x$)$_2$As$_2$

FIG. 3. For Ba(Fe$_{1-x}$Ag$_x$)$_2$As$_2$, temperature dependent normalized resistivity for $0 \leqslant x \leqslant 0.045$; the bottom inset has arbitrary ρ, and the top inset shows Hall coefficient for $x = 0, 0.019$, and 0.040.

For Ag-122, the T_N remains high and near 80 K at $x = 0.045$, in contrast to the fully suppressed AF and $T_c = 2$ K in Cu-122 at $x = 0.044$ or $T_N < 50$ K and $T_c = 15$ K in Co-122 at $x = 0.047$ [52].

The electrical transport measurements were performed in a QD Physical Property Measurement System (PPMS). Electrical leads were attached to the crystals using Dupont 4929 silver paste and resistivity measured in the ab plane in the range of 1.8 to 380 K. The ρ values at 380 K ranged from 0.1 to 1.2 mΩ cm, although their absolute values may have suffered from the geometry factor estimations. Figure 3 presents temperature-dependent normalized resistivity data; in the inset, the data set for each sample with composition x is shifted upward to clearly display transition anomalies. Electrical resistivity for 122 is as seen numerous times in literature, and the anomaly transition temperature (correspondent to T_N, T_S) is suppressed monotonically with increasing x, similar to literature [31–38]. The resistivity of the parent Ba-122 exhibits an abrupt decrease below the transition temperature. Despite the loss of carrier density, the decrease in the resistivity is due to a reconstruction of the Fermi surface in the orthorhombic striped-AF phase that generates high-mobility carriers dominating the charge transport [53,54]. For the lightly Ag-doped composition of $x = 0.005$, the anomaly manifests an abrupt resistivity peak around 122 K, similar to that found in Ba(Fe$_{0.9923}$Cu$_{0.0077}$)$_2$As$_2$ [37], followed by a decrease with cooling. For $x = 0.009$, the anomaly displays an increase around 112 K, followed by an almost flat resistivity dependence below. The resistivity for $x \geqslant 0.016$ first decreases gently from 380 K, followed by upturns below 106 K for $x = 0.016, 101$ K for $x = 0.019$, and 79 K for $x = 0.040$. Such upturns below the anomaly temperature and continued increase of ρ with decreasing temperature are similar to what occurs in other electron-doped crystals [10,36–38]. The upturn reflects the loss of carriers as a partial SDW gap opens below T_N. At temperatures well below T_N, the increase in the mobility of the remaining carriers is not enough to overcome the lower carrier concentration,

and the resistivity continues to increase. For $x = 0.045$, the transition is too weak to be observed, similar to that seen in magnetic-susceptibility behavior. The inferred transition temperatures were extracted by the derivative of resistivity curve ($d\rho/dT$) and are summarized in Table I. In the entire doping series of Ag-122, no drop to zero resistivity is seen up to the chemical doping limit. This is in contrast to all other transition-metal electron-doped 122, such as in Co [10], Ni [36], Rh [38], Pd [38], Ir [42], Pt [40,41], Cu [37], and Au [49], which give superconductivity in the comparable x regions.

In order to gain more insight into the evolution of transport properties, the temperature dependence of hall coefficient (R_H) for $x = 0, 0.019$, and 0.040 is presented in the upper inset of Fig. 3. The R_H of pure BaFe$_2$As$_2$ is negative in the temperature region of 10–300 K and shows a sharp decrease at the structural/magnetic transition near 132 K, as reported before [55]. The values of R_H for $x > 0$ are also negative between 10 and 300 K, with features at 100 K for $x = 0.019$ and ~ 80 K for $x = 0.040$, consistent with the Fermi surface gapping scenario for T_N [53,54]. These anomalies are coincident with inferred transitions in $\chi(T)$ and $\rho(T)$. The overall change of Hall data for $x = 0.019$ and 0.040 are not as rapid as 122, which signify a weaker electronic structure change and potentially reduced magnetism. The widths of transitions for $x = 0.040$ are more broad than $x = 0$ and 0.019. The values of R_H for $x = 0.019$ and 0.040 are less negative than that of parent 122 in the low temperature range. The negative sign of R_H indicates that electrons give the dominant contribution to the charge transport in 122 and Ag-doped 122s, and further analysis is complicated by multiband nature of the system and the presence of both electron and hole bands at the Fermi level.

Specific heat data were measured also using a PPMS, shown in Fig. 4. For 122, a sharp transition is observed at 132 K, as expected, for overlapping T_N and T_S. With Ag doping, the transition temperatures decrease monotonically, and the anomalies change from sharp peaks to broadened

FIG. 4. For Ba(Fe$_{1-x}$Ag$_x$)$_2$As$_2$, heat capacity for $0 \leqslant x \leqslant 0.045$ between 50 K and 150 K; the inset shows normalized dC/dT around the transitions.

features. Such a broadening feature is comparable to Cu-122 [37] and Au-122 [49]. The dC/dT is plotted in the left upper inset of Fig. 4 to show the transition temperatures. For $x = 0.005, 0.009, 0.016$, and 0.026, the anomalies occur at 120, 111, 105, and 92 K, respectively. There is no detectable transition in the $C(T)$ curve for $x = 0.045$, which suggests its weak nature or highly disordered/strained crystals. The extrapolated linear fit value of the C/T vs T^2 to zero, labeled as γ, for all the compositions is estimated to be between 6 and 16 mJ mol^{-1} K^{-2}. This weak change in γ with x is similar to that observed for Ba(Fe$_{1-x}$Au$_x$)$_2$As$_2$ and Ba(Fe$_{1-x}$Mo$_x$)$_2$As$_2$ [49,34], as may be expected for such low-doping levels. Moreover, the slightly doped Ba(Fe$_{1-x}$Co$_x$)$_2$As$_2$) (for $x = 0.045, \gamma \sim 14$ mJ mol^{-1} K^{-2}) also has a weak change in γ [56].

Single crystal neutron diffraction was performed using the four-circle diffractometer HB-3A at the High Flux Isotope Reactor (HFIR) at the Oak Ridge National Laboratory to distinguish between the structural and magnetic transitions for $x = 0, 0.005, 0.029, 0.035$, and 0.045. The neutron wavelength of 1.542 Å was used from a bent perfect Si-220 monochromator [57]. According to neutron diffraction data (Fig. 5), for 122 and as found before, there is a simultaneous structural and magnetic transition. In the magnetic state, the spins are aligned along a axis; the nearest-neighbor (NN) spins are antiparallel along a and c and are parallel along the shortest b axis. The nesting ordering wave vector is $q = (101)_O$ or $(\frac{1}{2}\frac{1}{2}1)_T$, relative to the tetragonal (T) or orthorhombic (O) nuclear cells [58]. In the top panels, the order parameter to the SDW order is seen by the intensity of the magnetic reflection $(105)_O/(\frac{1}{2}\frac{1}{2}5)_T$; for tracking T_S, the intensity of the $(400)_O/(220)_T$ nuclear peak was measured with warming. Similar to 122, the nuclear $(220)_T$ is expected to split to $(400)_O$ and $(040)_O$ orthorhombic Bragg reflections below T_S in Ag-122. The increased intensity of structural peak is due to reduced extinction effect by the structural transition from the tetragonal to orthorhombic lattice. The temperature dependence of the full width at half maximum (FWHM) peak of $(400)_O/(220)_T$ is shown in the bottom panels of Fig. 5; the peak broadening indicates the splitting of the $(220)_T$ peak. For Ag-122, we surprisingly find evidence that the magnetic and structural transitions occur roughly at the same temperature, i.e., $T_N = T_S = 125$ K for $x = 0.05$, $T_N = T_S = 84$ K for $x = 0.029$, and $T_N = T_S = 80$ K for both $x = 0.035$ and 0.045. Such behavior that T_N and T_S are coupled is different from behavior of Cu- or Au- dopants in 122 [37,49,59] or any other transition-metal electron-doped systems.

Based on the measurement results presented above, the $T-x$ phase diagram is constructed for the Ag-122 system, shown in Fig. 6. Upon Ag doping, the structural and magnetic transition temperatures decrease monotonically. Unlike other electron-doped 122s, T_N and T_S values coincide for Ag-122 without splitting. This phase diagram is clearly divided into two regions: the tetragonal NM (TET/NM) and the orthorhombic AFM (ORTH/AFM). The comparisons of T_N vs x for Ag- and Cu-122 are illustrated in the inset of Fig. 6. For Cu-122, superconductivity with $T_c \sim 2$ K was found in the $x = 0.044$ sample, and T_N suppressed linearly with x. For Ag-122 and for $x \leqslant 0.019$, T_N follows the same guideline as Cu-122, while for $x > 0.019$, it starts to deviate approaching a potentially saturated value (of 78 K) around $x = 0.045$. This
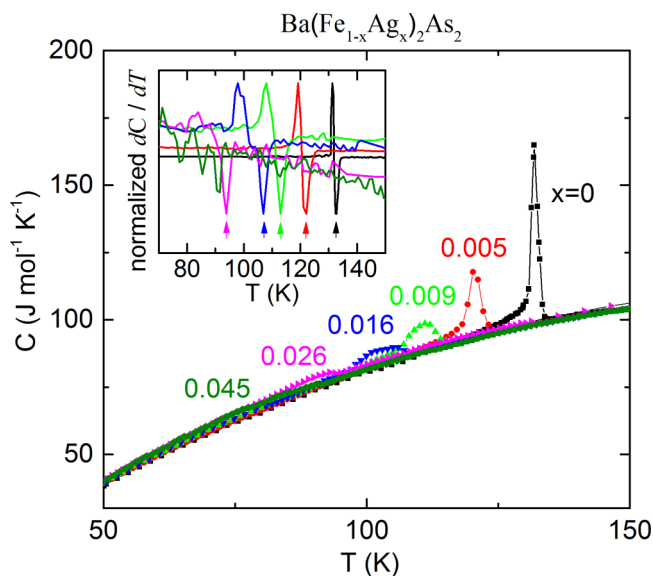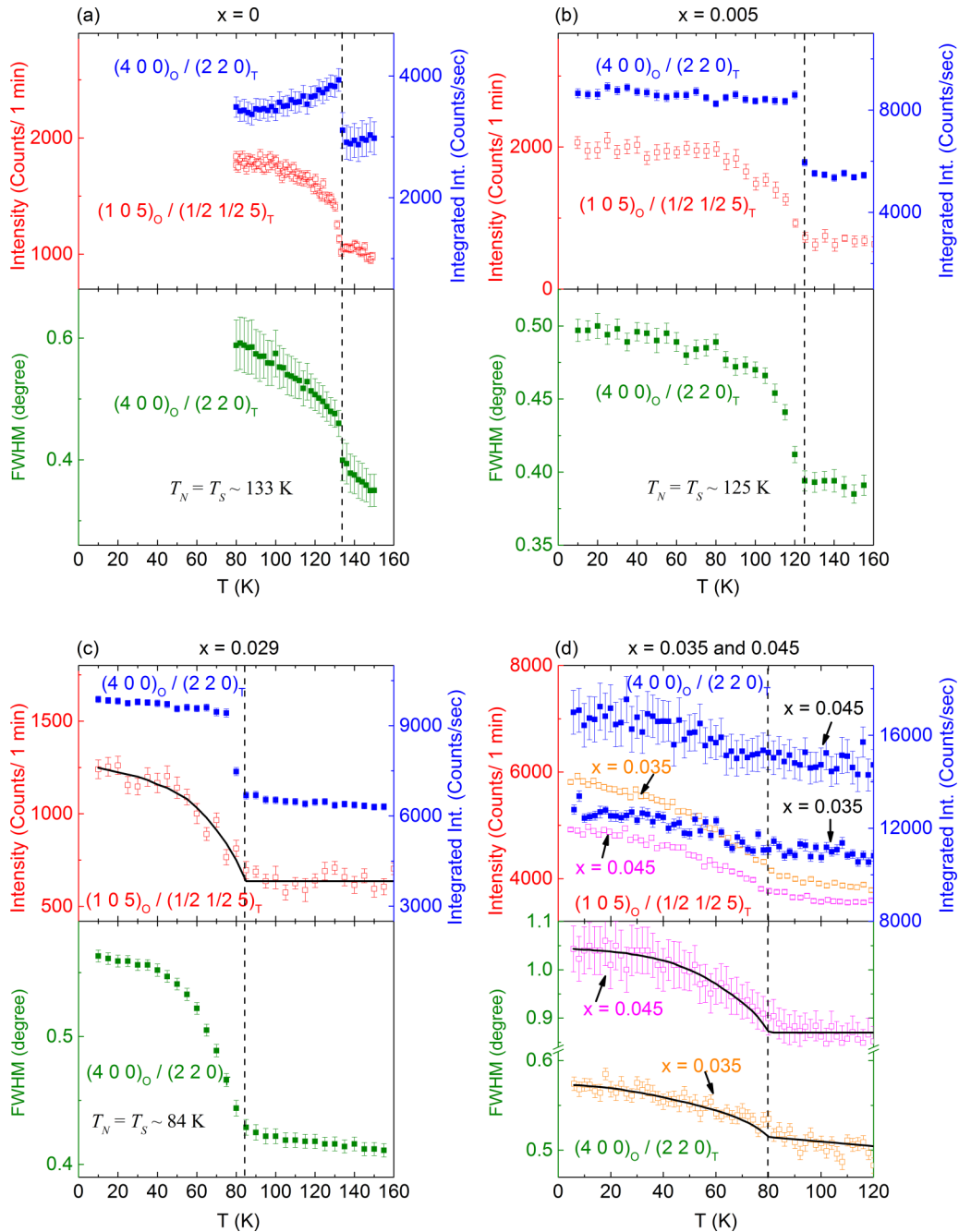
FIG. 5. For $Ba(Fe_{1-x}Ag_x)_2As_2$ crystals, neutron diffraction results for $x = 0, 0.005, 0.029, 0.035,$ and 0.045. The temperature dependence of Bragg reflection results upon warming. Top panels: integrated intensity of the nuclear peak $(400)_O/(220)_T$ and the peak intensity of the magnetic peak $(105)_O/(\frac{1}{2}\frac{1}{2}5)_T$; curved line is a guide for eyes. The solid/dashed line marks the structural/magnetic transition. Bottom panels: full peak width of $(400)_O/(220)_T$ at half peak maximum. The nonzero intensity of the magnetic peak above T_N is from the neutron background and 1.5% half wavelength beam contamination and does not change with temperature.

deviation in T_N corresponds to those in c lattice parameters and crystal features, and it may imply some change for the distance and interaction between FeAs layers that play an important role for persisting magnetism in Ag-122.

III. THEORETICAL CALCULATIONS

In an attempt to understand the observed behavior, in particular, the lack of superconductivity and maintenance

of a magnetic state for Ag-122, we have performed first principles density functional theory calculations using the commercially available all-electron code WIEN2k [60] within the local density approximation (LDA). We have chosen the LDA rather than the generalized gradient approximation (GGA) as it may give a better account of properties in 122s. There are two basic effects that must be considered in these calculations—the effect of *electron count* or charge doping, and the effects of *strain*— the change in structural parameters
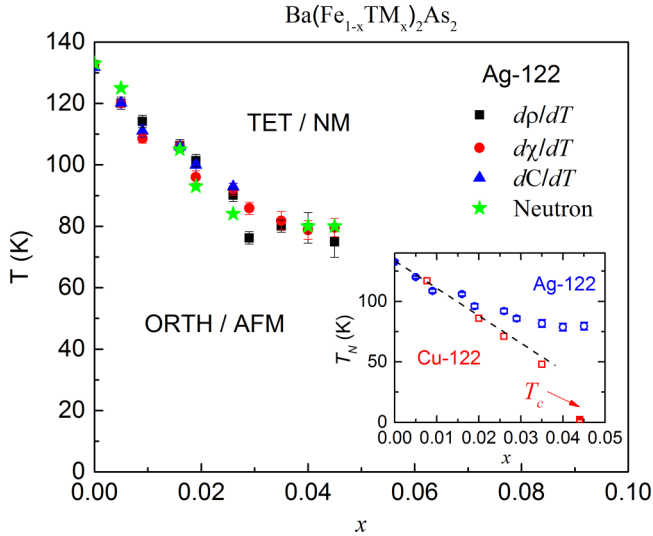
FIG. 6. The $T - x$ phase diagram for Ag-122. Inset shows T_N vs x for Ag-122 and Cu-122 (data retrieved from Ref. [37]).

FIG. 7. The calculated DOSs for Ba-122 doped with each of the indicated dopants.

such as lattice constants with doping. In order to properly account for these effects, we have performed calculations in the tetragonal unit cell with one of the four equivalent Fe atoms substituted by Ag, Cu, Co, or Mn, using the room temperature structural parameters for 122 doped with each of these at $x \sim 0.04$. Note that the experimental observations for 122 with each of these dopants are very different: Ag doping produces *no* superconductivity, Cu produces a very slight superconductivity with maximum T_c of 2 K, Co doping produces a substantial superconducting dome with T_c values of 20 K, and Mn produces no superconductivity. What is the reason for these disparate behaviors? To answer this question, in this paper we consider the impact of the dopant on electronic scattering. Such scattering has long been known to negatively impact superconductivity. One measure of such scattering, as described in [10], is the effective disruption of the electronic structure occasioned by the dopant atom. To the extent that the states arising from the dopant atom mirror those of the overall system, both in their energy range and magnitude, one may expect that such a dopant introduces charge without inordinate electronic scattering and thus might induce superconductivity. On the other hand, a dopant that induces an energetically distinct set of electronic states can reasonably be expected to create large scattering and thus be less likely to induce (or allow) superconductivity. The simplest way to access this is through examination of the calculated DOSs.

We depict the results of these calculations in Fig. 7. The top panel shows the result for Ag doping. We see that the Ag creates essentially a band separate from the rest of the electronic states, falling between 5.5 and 7.5 eV below the Fermi energy. This is a wholesale disruption of the electronic structure and is indicative of intense electronic scattering, consistent with the lack of superconductivity in Ag-122. It is instructive to compare the Ag results to the Cu results. In this latter case, the Cu states, unlike the Ag states, do not form a separate band but fall broadly within a range 1.5 to 6 eV below E_F. While there is still substantial scattering associated with this band (it does not mirror the
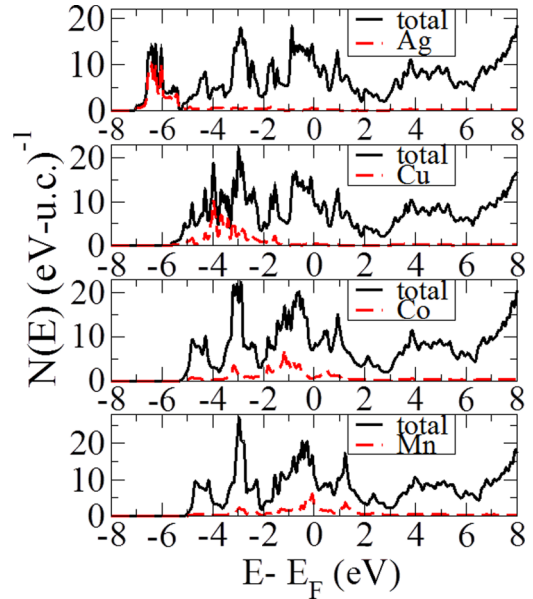
overall DOS), it is likely to be significantly less than for Ag doping, suggesting the possibility of superconductivity for Cu doping. It is instructive to consider the last two results—for Co and Mn doping. The Co-doped DOS shows significantly less disruption than either Ag or Cu—the Co states fall within a wide range from -4 eV to $+1$ eV—and the maximum Co DOS at -1.1 eV is not far from the overall DOS maximum at -0.6 eV. In fact, Co-122 has a larger superconducting dome ($T_{c,\max} \approx 22$ K and $\Delta x = 0.1$) than Cu-122 ($T_{c,\max} = 2$ K and $\Delta x = 0.015$) [37,55]. Hence, the electronic scattering is still less here, again generally consistent with the substantial superconducting dome for Co doping. Surprisingly, of the four dopants considered, the dopant that produces the least disruption to the electronic structure is Mn. Here, the DOS generally mirrors the overall electronic structure for a wide range around E_F. In this range, its value is near the $\frac{1}{4}$ ratio of the total DOS that would indicate no disruption, and no separate band, as in the case of Ag, is visible. Experimentally, Mn doping produces no superconductivity but rather yields a magnetic ground state, which is likely due to the tendency of Mn to retain a distinct local moment. An additional effect, not considered here, is magnetic scattering, which one would expect to be intense for Mn doping. However, this DOS result does suggest some possibility for achieving superconductivity via hole doping of the Fe site, which has never been achieved. Therefore, one possible explanation for the maintenance of magnetism in Ag-122 can be found in the Fermi-level DOSs for the four supercells—Ag, Cu, Co, and Mn. Respectively, these values (per Rydberg-unit cell) are 145.4, 133.4, 103.3, and 136.0, so that in fact the Fermi level DOS is *highest* for Ag doping. Given that magnetism in these families results partly from Stoner physics [61], in which high DOSs play a key role, it is possible that details of the Ag-Fe interaction cause this interaction to be *less* disruptive to magnetism than for other dopants. We note that the Co-doped cell, which produces the largest superconducting dome, shows the lowest Fermi-level

DOS and so might be considered more effective at disrupting the magnetic state and allowing superconductivity to emerge. Further consideration of this topic will be in our future work.

In conclusion, this paper is the first study of silver substitution in BaFe$_2$As$_2$. We represent the $T - x$ phase diagram through extended experimental work. Comparing 4d Ag-122 to 3d Cu- and 5d Au- dopants of the same group, similar suppression of T_N is seen up to 2% Ag substitution. However, as the doping level increases, Cu- and Au-122 give superconductivity at $\sim$2 K at 4.4% and 3.1% doping level, respectively, and Ag remains magnetic up to *5% doping*. Our theoretical calculations suggest that Ag substitution produces strong electronic scattering and yet a relatively small disruption of the magnetic state, both of which preclude superconductivity in this system.

[1] J. G. Bednorz and K. A. Müller, Z. Phys. B Condens. Matter **64**, 189 (1986).

[2] Y. Kamihara, T. Watanabe, M. Hirano, and H. Hosono, J. Am. Chem. Soc. **130**, 3296 (2008).

[3] A. S. Sefat and D. J. Singh, MRS Bull. **36**, 614 (2011).

[4] I. I. Mazin, Nature **464**, 183 (2010).

[5] M. D. Lumsden and A. D. Christianson, J. Phys. Condens. Matter **22**, 203203 (2010).

[6] A. S. Sefat, Rep. Prog. Phys. **74**, 124502 (2011).

[7] P. Dai, J. Hu, and E. Dagotto, Nat. Phys. **8**, 709 (2012).

[8] G. R. Stewart, Rev. Mod. Phys. **83**, 1589 (2011).

[9] A. V. Chubukov, D. V. Efremov, and I. Eremin, Phys. Rev. B **78**, 134512 (2008).

[10] A. S. Sefat, R. Jin, M. A. McGuire, B. C. Sales, D. J. Singh, and D. Mandrus, Phys. Rev. Lett. **101**, 117004 (2008).

[11] R. M. Fernandes, A. V. Chubukov, and J. Schmalian, Nat. Phys. **10**, 97 (2014).

[12] I. Mazin, Physics **4**, 26 (2011).

[13] J. Paglione and R. L. Greene, Nat. Phys. **6**, 645 (2010).

[14] P. M. Aswathy, J. B. Anooja, P. M. Sarun, and U. Syamaprasad, Supercond. Sci. Technol. **23**, 73001 (2010).

[15] A. Gurevich, Rep. Prog. Phys. **74**, 124501 (2011).

[16] A. A. Kordyuk, Low Temp. Phys. **38**, 888 (2012).

[17] S. A. Kivelson and H. Yao, Nat. Mater. **7**, 927 (2008).

[18] H.-H. Wen, Adv. Mater. **20**, 3764 (2008).

[19] K. Tanabe and H. Hosono, Jpn. J. Appl. Phys. **51**, 10005 (2012).

[20] J. C. Davis and P. J. Hirschfeld, Nat. Phys. **10**, 184 (2014).

[21] X. Chen, P. Dai, D. Feng, T. Xiang, and F.-C. Zhang, Natl. Sci. Rev. **1**, 371 (2014).

[22] J. W. Lynn and P. Dai, Phys. C Supercond. **469**, 469 (2009).

[23] A. S. Sefat, Curr. Opin. Solid State Mater. Sci. **17**, 59 (2013).

[24] K. Ishida, Y. Nakai, and H. Hosono, J. Phys. Soc. Jpn. **78**, 62001 (2009).

[25] D. C. Johnston, Adv. Phys. **59**, 803 (2010).

[26] D. J. Singh, Phys. C Supercond. **469**, 418 (2009).

[27] P. Richard, T. Sato, K. Nakayama, T. Takahashi, and H. Ding, Rep. Prog. Phys. **74**, 124512 (2011).

[28] P. J. Hirschfeld, M. M. Korshunov, and I. I. Mazin, Rep. Prog. Phys. **74**, 124508 (2011).

[29] A. Chubukov and P. J. Hirschfeld, Phys. Today **68**, 46 (2015).

[30] M. Rotter, M. Tegel, D. Johrendt, I. Schellenberg, W. Hermes, and R. Pöttgen, Phys. Rev. B **78**, 020503 (2008).

[31] A. S. Sefat, M. A. McGuire, R. Jin, B. C. Sales, D. Mandrus, F. Ronning, E. D. Bauer, and Y. Mozharivskyj, Phys. Rev. B **79**, 094508 (2009).

[32] A. S. Sefat, D. J. Singh, L. H. VanBebber, Y. Mozharivskyj, M. A. McGuire, R. Jin, B. C. Sales, V. Keppens, and D. Mandrus, Phys. Rev. B **79**, 224524 (2009).

[33] M. G. Kim, A. Kreyssig, A. Thaler, D. K. Pratt, W. Tian, J. L. Zarestky, M. A. Green, S. L. Bud'ko, P. C. Canfield, R. J. McQueeney, and A. I. Goldman, Phys. Rev. B **82**, 220503 (2010).

[34] A. S. Sefat, K. Marty, A. D. Christianson, B. Saparov, M. A. McGuire, M. D. Lumsden, W. Tian, and B. C. Sales, Phys. Rev. B **85**, 024503 (2012).

[35] K. Marty, A. D. Christianson, C. H. Wang, M. Matsuda, H. Cao, L. H. VanBebber, J. L. Zarestky, D. J. Singh, A. S. Sefat, and M. D. Lumsden, Phys. Rev. B **83**, 060509 (2011).

[36] A. S. Sefat, D. J. Singh, R. Jin, M. A. McGuire, B. C. Sales, F. Ronning, and D. Mandrus, Phys. C Supercond. **469**, 350 (2009).

[37] N. Ni, A. Thaler, J. Q. Yan, A. Kracher, E. Colombier, S. L. Bud'ko, P. C. Canfield, and S. T. Hannahs, Phys. Rev. B **82**, 024519 (2010).

[38] N. Ni, A. Thaler, A. Kracher, J. Q. Yan, S. L. Bud'ko, and P. C. Canfield, Phys. Rev. B **80**, 024511 (2009).

[39] P. C. Canfield and S. L. Bud'ko, Annu. Rev. Condens. Matter Phys. **1**, 27 (2010).

[40] X. Zhu, F. Han, G. Mu, P. Cheng, J. Tang, J. Ju, K. Tanigaki, and H.-H. Wen, Phys. Rev. B **81**, 104525 (2010).

[41] Y. Guo, X. Wang, J. Li, S. Zhang, K. Yamaura, and E. Takayama-Muromachi, J. Phys. Soc. Jpn. **81**, 64704 (2012).

[42] X. L. Wang, H. Y. Shi, X. W. Yan, Y. C. Yuan, Z.-Y. Lu, X. Q. Wang, and T.-S. Zhao, Appl. Phys. Lett. **96**, 12507 (2010).

[43] D. K. Pratt, W. Tian, A. Kreyssig, J. L. Zarestky, S. Nandi, N. Ni, S. L. Bud'ko, P. C. Canfield, A. I. Goldman, and R. J. McQueeney, Phys. Rev. Lett. **103**, 087001 (2009).

[44] S. Nandi, M. G. Kim, A. Kreyssig, R. M. Fernandes, D. K. Pratt, A. Thaler, N. Ni, S. L. Bud'ko, P. C. Canfield, J. Schmalian, R. J. McQueeney, and A. I. Goldman, Phys. Rev. Lett. **104**, 057006 (2010).

[45] X. Lu, H. Gretarsson, R. Zhang, X. Liu, H. Luo, W. Tian, M. Laver, Z. Yamani, Y.-J. Kim, A. H. Nevidomskyy, Q. Si, and P. Dai, Phys. Rev. Lett. **110**, 257001 (2013).

[46] A. Kreyssig, M. G. Kim, S. Nandi, D. K. Pratt, W. Tian, J. L. Zarestky, N. Ni, A. Thaler, S. L. Bud'ko, P. C. Canfield, R. J. McQueeney, and A. I. Goldman, Phys. Rev. B **81**, 134512 (2010).

[47] M. P. M. Dean, M. G. Kim, A. Kreyssig, J. W. Kim, X. Liu, P. J. Ryan, A. Thaler, S. L. Bud'ko, W. Strassheim, P. C. Canfield, J. P. Hill, and A. I. Goldman, Phys. Rev. B **85**, 140514 (2012).

[48] M. G. Kim, D. K. Pratt, G. E. Rustan, W. Tian, J. L. Zarestky, A. Thaler, S. L. Bud'ko, P. C. Canfield, R. J. McQueeney, A. Kreyssig, and A. I. Goldman, Phys. Rev. B **83**, 054514 (2011).

[49] L. Li, H. Cao, M. A. McGuire, J. S. Kim, G. R. Stewart, and A. S. Sefat, Phys. Rev. B **92**, 094504 (2015).

[50] R. D. Shannon, Acta Crystallogr. Sect. A **32**, 751 (1976).

[51] B. C. Sales, M. A. McGuire, A. S. Sefat, and D. Mandrus, Phys. C Supercond. **470**, 304 (2010).

[52] N. Ni, M. E. Tillman, J.-Q. Yan, A. Kracher, S. T. Hannahs, S. L. Bud'ko, and P. C. Canfield, Phys. Rev. B **78**, 214515 (2008).

[53] S. Ishida, T. Liang, M. Nakajima, K. Kihou, C. H. Lee, A. Iyo, H. Eisaki, T. Kakeshita, T. Kida, M. Hagiwara, Y. Tomioka, T. Ito, and S. Uchida, Phys. Rev. B **84**, 184514 (2011).

[54] T. Terashima, N. Kurita, M. Tomita, K. Kihou, C.-H. Lee, Y. Tomioka, T. Ito, A. Iyo, H. Eisaki, T. Liang, M. Nakajima, S. Ishida, S. I. Uchida, H. Harima, and S. Uji, Phys. Rev. Lett. **107**, 176402 (2011).

[55] E. D. Mun, S. L. Bud'ko, N. Ni, A. N. Thaler, and P. C. Canfield, Phys. Rev. B **80**, 054517 (2009).

[56] K. Gofryk, A. S. Sefat, M. A. McGuire, B. C. Sales, D. Mandrus, J. D. Thompson, E. D. Bauer, and F. Ronning, Phys. Rev. B **81**, 184518 (2010).

[57] B. C. Chakoumakos, H. Cao, F. Ye, A. D. Stoica, M. Popovici, M. Sundaram, W. Zhou, J. S. Hicks, G. W. Lynn, and R. A. Riedel, J. Appl. Crystallogr. **44**, 655 (2011).

[58] Q. Huang, Y. Qiu, W. Bao, M. A. Green, J. W. Lynn, Y. C. Gasparovic, T. Wu, G. Wu, and X. H. Chen, Phys. Rev. Lett. **101**, 257003 (2008).

[59] H. Takeda, T. Imai, M. Tachibana, J. Gaudet, B. D. Gaulin, B. I. Saparov, and A. S. Sefat, Phys. Rev. Lett. **113**, 117001 (2014).

[60] P. Blaha, K. Schwarz, G. Madsen, D. Kvasnicka and J. Luitz, *WIEN2k, An Augmented Plane Wave + Local Orbitals Program for Calculating Crystal Properties* (Karlheinz Schwarz, Techn. Universität Wien, Austria, 2001).

[61] D. J. Singh and M.-H. Du, Phys. Rev. Lett. **100**, 237003 (2008).